6-1987

Collisions of F+ with Ne

M. Hottoka

B. Roos

John B. Delos
William & Mary, jbdelo@wm.edu

R. Srivastava

R. B. Sharma

See next page for additional authors

Recommended Citation

Hottoka, M.; Roos, B.; Delos, John B.; Srivastava, R.; Sharma, R. B.; and Koshi, W., Collisions of F+ with Ne (1987). *Physical Review A*, 35(11), 4515-4525.
https://doi.org/10.1103/PhysRevA.35.4515

Collisions of F^+ with Ne

Matti Hottoka and Björn Roos
Division of Physical Chemistry, University of Lund, 522007 Lund, Sweden

J. B. Delos*
Physics Department, College of William and Mary, Williamsburg, Virginia 23185

R. Srivastava
Physics Department, University of Roorkee, Roorkee, India

R. B. Sharma and W. S. Koski
Chemistry Department, Johns Hopkins University, Baltimore, Maryland 21218
(Received 16 December 1986)

Measurements of inelastic collisions of F^+ with Ne have been made. Transitions between ^3P and ^1D terms of F^+ are seen, with the inelastically scattered ions sharply focused in the forward direction. Potential energy curves of $(FNe)^+$ have been calculated. The $^3\Sigma$ and $^3\Pi$ curves correlating to $F^+(^3P)$ are repulsive, while the $^1\Sigma$ correlating to $F^+(^1D)$ is attractive. Several curve crossings are identified, where transitions occur through spin-orbit coupling. Scattering angles and differential cross sections have been calculated, and they show the presence of a "glory" (or halo) effect, which accounts for the forward scattering of ions.

I. INTRODUCTION

The formation and deexcitation of neutral rare-gas—halide molecules have been extensively investigated.[1–6] Similarly, experimental and theoretical studies have been carried out on rare-gas oxides, because of the potential application of these systems in lasers.[7,8] On the other hand, there has been only a very limited number of studies on the rare-gas—halide diatomic ions. These rare-gas—halogen positive-ion systems are isoelectronic with the rare-gas oxides, and as such, they might also be suitable candidates for laser systems.

In addition, rare gases have been used as moderators in hot-atom studies of halogens, and generally the assumption has been made in these studies that the rare gases are inert. Recently, however, it has been demonstrated that this assumption is not applicable to halogen hot-atom systems: collisional studies between Br^+ and Kr show that Kr is not inert, but participates in an active chemical way in the hot-atom process.[9]

In the 1960s, with the discovery of stable xenon and krypton fluorides, it was shown by mass spectroscopic techniques that XeF^+ and KrF^+ are stable ions.[10] The noble-gas—halide ions, $KrCl^+$, KrF^+, $ArCl^+$, and ArI^+ have been reported as stable ions.[11,12] The raw $KrBr^+$ has been prepared and its dissociation energy inferred from a threshold measurement of collision dissociation reactions.[13] ArF^+ has been reported to have a dissociation energy of ≥ 1.655 eV.[14] On the other hand, attempts to make NeF^+ and HeF^+ have been unsuccessful.[14]

In order to get better insight into the nature of the diatomic rare-gas—halide ions, we are investigating the collisions between halogen positive ions and rare-gas atoms. At this time, we report our results on the Ne-F^+ system.

An energy-level diagram of the Ne-F^+ system at infinite interatomic separation is shown in Fig. 1. Since the maximum kinetic energy involved in our excitation experiments was only 10 eV, no states other than the ones shown are energetically accessible. Our experiments deal mainly with excitation and deexcitation,

$$F^+(^3P)+Ne(^1S)\rightleftarrows F^+(^1D)+Ne(^1S)\ , \tag{1}$$

and with charge transfer

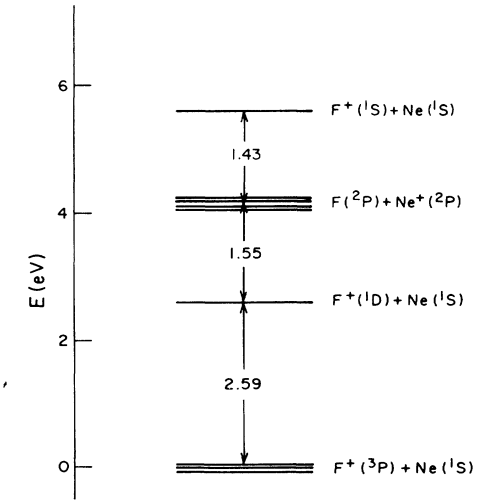

FIG. 1. Energy levels for $F^+ + Ne$ and $F + Ne^+$ at infinite separation. Energy gaps in eV are indicated, with spin-orbit splittings greatly exaggerated.

$$F^+(^3P \text{ or } ^1D) + Ne(^1S) \rightleftarrows F(^2P) + Ne^+(^2P) , \quad (2)$$

both of which are indicated in Fig. 1.

II. EXPERIMENTAL RESULTS

A. Inelastic scattering

Collisions of F^+ with Ne were measured using a tandem mass spectrometer which has been described previously.[15] It consists of an ion source, an electrostatic analyzer, and a quadrupole mass spectrometer as an input section. The ions were prepared by electron bombardment of CH_3F. The beam composition so produced had 30% $F^+(^1D_2)$ and 70% $F^+(^3P_{0,1,2})$, as determined by attenuation measurements of the F^+ in neon.[16] The beam width was 0.1 eV in energy and 1.5° in angle [both full width at half maximum (FWHM)].

The beam of F^+ ions from this section was passed through a shallow reaction chamber containing the target gas Ne. The ions scattered to 0° to the beam direction were then detected with a second quadrupole mass spectrometer followed by an electrostatic analyzer and an electron multiplier.

In this way, an energy spectrum of forward-scattered F^+ was obtained (Fig. 2). The central peak is the unperturbed F^+. The satellite peaks on each side of the primary are separated by 2.6 eV from the main peak. The spacing between the $^3P_2$ ground state of F^+ and the first excited state $^1D_2$ is 2.587 eV, so we interpret these peaks as representing the process (1). The "superelastic" peak on the right corresponds to the transition $F^+(^1D_2) \rightarrow F^+(^3P_{0,1,2})$ and the more intense "subelastic" satellite on the left is due to the transition $F^+(^3P_{0,1,2}) \rightarrow F^+(^1D_2)$. [Spacings of the spin-orbit energy levels ($J=0,1,2$) are too small to be resolved.] At incident kinetic energies below 2.5 eV (c.m.), the left-hand peak was not detected.

We shall explain later that this inelastic process results from spin-orbit coupling. Because this magnetic effect is very weak, it is rather surprising that a substantial current of excited or deexcited ions is seen. To examine it further, we measured the angular distribution of inelastically scattered F^+. This is shown in Fig. 3. This graph was obtained in the following manner. The detector was set at an angle relative to the incident beam (0°, $\frac{1}{2}$°, 1°, . . . , 5°), and at each angle an energy scan gave result similar to Fig. 2. The largest value of scattered current in the satellite peaks was recorded and plotted in Fig. 3.

We see that the inelastic products are very sharply focused in the forward direction. The inelastic current decreases by a factor of 10 within 3° from the forward direction, and the FWHM of the scattered current is similar to that of the primary beam. Such sharp forward peaking of an inelastically scattered product is a very unusual phenomenon in an ion-atom collision.

B. Search for $(NeF)^+$

In view of the fact that the rare-gas diatomic halide ions $ArCl^+$, $KrBr^+$, and XeI^+ are easily prepared by electron bombardment of a mixture of the rare gas and halogen molecule, we carried out similar experiments on Ne-F_2 mixtures. Mass spectroscopic analysis of the mixture clearly showed a mass-39 peak which may correspond to NeF^+. However, the intensity was not sufficiently high to carry out corroborative experiments (such as collision-induced dissociation) to support the peak assignment. In this connection it is interesting to note that Berkowitz and Chupka[14] were not successful in producing NeF^+ by the reaction of $F_2^+(Ne,F)NeF^+$.

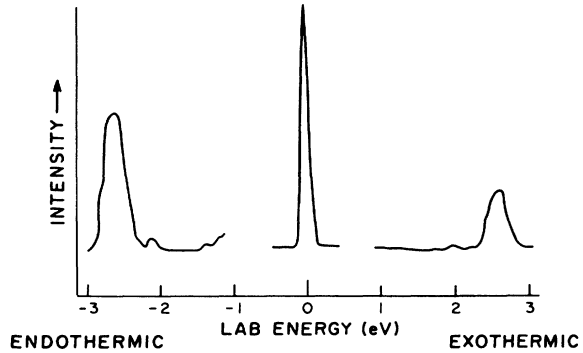

FIG. 2. Current of subelastic and superelastic F^+ scattered in the forward direction. The peaks occur at ±2.6 eV, indicating that $^3P \leftrightarrow {}^1D$ excitation and deexcitation are occurring.

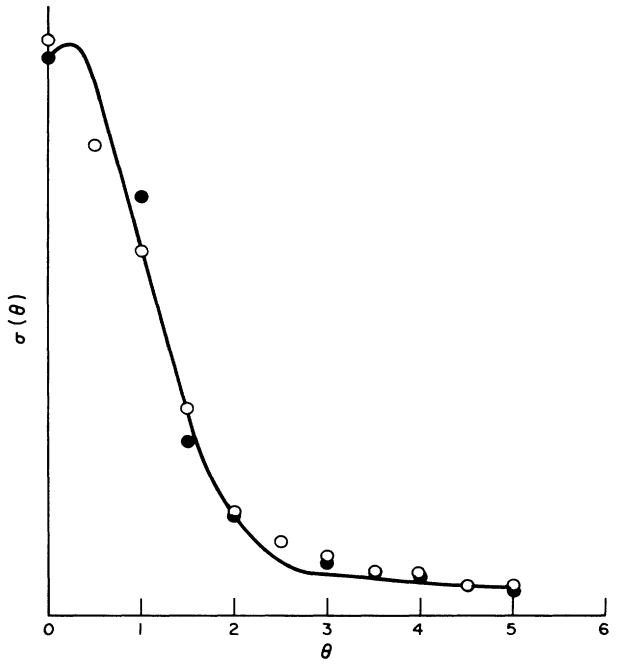

FIG. 3. Angular distribution of inelastically scattered F^+. Open circles: 2.6 eV endothermic; solid circles: 2.6 eV exothermic. The inelastic process is concentrated in the forward direction. Solid line: calculation discussed in Sec. V. [In principle the units of $\sigma(\theta)$ are bohrs^2/steradian, but only the *relative* differential cross section is measured.]

C. Charge transfer

To complete our discussion of experimental results, let us recall the results of charge-transfer experiments reported earlier.[16] In these experiments, the F^+ ion beam was produced by electron bombardment of CF_4. Evidence was presented[16] that the beam contained a mixture of ^1D and ^3P states; however, when NO was added to the CF_4 then the excited states were quenched, and the F^+ beam contained only the ground ^3P state. The total charge-transfer cross section was measured by collecting product Ne^+ ions for the mixed beam (^1D and ^3P), and for the ground state (^3P) beam, and in this way the two total cross sections for process (2) were inferred.

The ground-state total charge-transfer cross section for $F^+(^3P)+Ne\rightarrow F+Ne^+$ has a threshold near 4 eV (c.m.), consistent with the energy-level diagram (Fig. 1), and it has a maximum of about 4 $Å^2$ for F^+ kinetic energies around 20 eV (c.m.). For the excited state, $F^+(^1D)+Ne\rightarrow F+Ne^+$, the threshold is below 2 eV, and the maximum cross section is about 12 $Å^2$ at an energy of about 8 eV (c.m.).

D. Summary

To summarize the experimental results, we have seen unambiguous evidence of the inelastic processes (1). The current of inelastically scattered particles is small, and sharply peaked in the forward direction. The total charge-transfer cross section has already been measured and it is substantial (5–10 $Å^2$). Finally, some (inconclusive) evidence was found for the existence of stable or metastable $(NeF)^+$.

III. ELECTRONIC ENERGIES OF $(NeF)^+$

To interpret these results, it is necessary to have some knowledge of the Ne-F^+ potential energy curves. In this section we present the results of quantum-chemical calculations of these curves.

A. Computational details

Ab initio calculations were performed using the complete active space self-consistent-field (CAS-SCF) method in the "super-configuration-interaction (CI)" formulation.[17] In this multiconfiguration (MC) model the molecular orbital (MO) space is divided into inactive, active, and secondary subspaces. The orbitals in the inactive subspace are always doubly occupied. The remaining electrons are distributed in all possible ways among the MO's in the active subspace, resulting in a complete list of electron configurations within the active subspace. Therefore no list of configurations needs to be compiled in advance; the only step requiring chemical intuition is the choice of the active orbitals. The orbitals in the secondary subspace are always empty. Unitary rotations between the three orbital subgroups are performed until the condition for optimized MCSCF orbitals—the generalized Brillouin theorem—is satisfied.[18] Unitary-group methods[19] are used to compute the configuration-expansion coefficients in the multiconfiguration wave function.

In the present calculations the 1σ, 2σ, 3σ, and 4σ orbitals (i.e., essentially the $1s$ and $2s$ atomic orbitals of neon and fluorine) formed the inactive subspace. The active subspace consisted of the 5σ, 6σ, 1π, 2π, and 3π orbitals. Thus the active subspace contains the $2p$ shells of fluorine and neon plus one extra π orbital. This active subspace has previously been used for the F_2 molecule, and was in that case shown to give good results for the equilibrium properties and dissociation energy (cf. Table III and Ref. 20). The number of spin-adapted configurations obtained by distributing ten electrons among the active orbitals varied between 300 and 500 depending on the symmetry of the state. For technical reasons the calculations were performed using C_{2v} symmetry. An averaging procedure was used to keep the two components of the π orbitals equivalent, thus ensuring a correct linear symmetry of the total wave function.

The atomic Gaussian basis sets for neon and fluorine consisted of eleven s and seven p primitive functions,[21] contracted to six s and four p using the scheme (6,1,1,1,1,1;4,1,1,1), and augmented with two sets of polarization functions. The final d orbital exponents $\zeta_d(\mathrm{Ne})=2.70$, 0.78, and $\zeta_d(\mathrm{F})=2.72$, 0.68 were obtained by scaling the exponents suggested by Ahlrichs.[22] The optimal scaling factors were determined in a series of SCF calculations on the NeF^+ molecular ion at an interatomic distance of 2.4 a.u.

The spectroscopic characteristics of the bound states were obtained by solving numerically the rovibrational Schrödinger equation in the calculated potential curves. Four vibrational and twenty rotational states were used to fit the spectroscopic constants to the calculated rotational and vibrational energies. The rotational constants were obtained by fitting to the term values for each band, while the vibrational constants were obtained from a fit to the band origins.

B. Results and discussion

The NeF^+ system has the four low-lying dissociation limits shown in Fig. 1. These correlate with 18 molecular electronic states as indicated in Table I. In the present work we have determined potential energy curves for the lowest $^3\Pi$ and $^3\Sigma^-$ states, and those of the higher states that may cross or approach closely the two lowest ones, i.e., the $^1\Sigma^+$, $^1\Pi$, and $^1\Delta$ states dissociating into $Ne(^1S)+F^+(^1D)$ and the lowest $^1\Sigma^+$, $^3\Sigma^+$, $^1\Sigma^-$, $^1\Pi$, $^3\Pi$, and $^3\Delta$ states dissociating into $Ne^+(^2P)+F(^2D)$. In all, 11 out of the 18 possible potential curves were studied. The computed potential curves are given in Table II.

The asymptotic energies can be compared with the experimental energy levels of the atom and ion.[23] The excitation energy from $F^+(^2P)$ to $F^+(^1D)$ is calculated to be 2.84 eV, or 0.25 eV too high. Similarly, the distance to the $Ne^+(^2P)+F(^2P)$ state is calculated to be 4.31 or 0.17 eV above the experimental value. These small differences do not affect the calculated crossing points appreciably, as is seen in Table III. The curves shown in Fig. 4 have been shifted to the experimental asymptotic energies. (The tiny variations in the asymptotic energies of the states with the same dissociation limits in Table II are caused by differ-

TABLE I. Dissociation products and spectroscopic states for NeF^+.

States	Asymptote	Asymptotic energy (eV)[a]
$1\,^3\Sigma^-$, $1\,^3\Pi$	$Ne(^1S)+F^+(^3P)$	0.00 (0.00)
$1\,^1\Delta$, $1\,^1\Pi$, $1\,^1\Sigma^+$	$Ne(^1S)+F^+(^1D)$	2.84 (2.59)
$2\,^1\Sigma^+$, $3\,^1\Sigma^+$,		
$1\,^3\Sigma^+$, $2\,^3\Sigma^+$,		
$1\,^1\Sigma^-$, $2\,^3\Sigma^-$,	$Ne^+(^2P)+F(^2P)$	4.31 (4.14)
$2\,^3\Pi$, $3\,^3\Pi$,		
$2\,^1\Pi$, $3\,^1\Pi$.		
$2\,^1\Delta$, $1\,^3\Delta$		
$4\,^1\Sigma^+$	$Ne(^1S)+F^+(^1S)$	(5.57)

[a]Computed asymptotic relative energies; experimental values within parentheses (Ref. 22).

ences in the MC expansions in the different symmetries.)

Only two of the electronic states were found to be binding, the lowest $^1\Sigma^+$ and $^1\Pi$ states. The $^1\Sigma^+$ state has a dissociation energy of 1.644 eV and an equilibrium bond distance of 1.465 Å. Liebman and Allen[24] reported Hartree-Fock calculations on this state; they found an equilibrium bond distance of 1.65 Å and a dissociation energy of about 1.3 eV, in reasonable agreement with the present results. The strong binding in this state derives from the fact that the dominant F^+ configuration at small distances is $2p_x^2 2p_y^2$ (counting electrons) or $\overline{2p}_z^{\,2}$ (counting holes); the two empty $2p_z$ orbitals are aimed at the Ne atom, allowing strong binding to occur.

This $^1\Sigma^+$ curve is crossed by the $^3\Sigma^-$ and $^3\Pi$ curves correlating with $F^+(^3P)$, and spin-orbit coupling induces electronic transitions that would lead to dissociation. However, if these transitions are neglected, the rovibrational levels of NeF^+ can be calculated, and spectroscopic parameters can be determined as explained above. These spectroscopic parameters are presented in Table IV. For comparison, and to provide a test of the accuracy of the calculated potential curves, the corresponding parameters were calculated by the same method for the isoelectronic F_2 molecule. These are also presented in Table IV, together with the experimental values. The results obtained for F_2 are remarkably (in fact, fortuitously) good, and a close resemblance between these two isoelectronic molecules is found, as could be expected. Hence a roughly similar accuracy can be expected in the case of NeF^+, and therefore the choice of active subspace and atomic basis set seems adequate. This conclusion is corroborated by the relatively small errors in the asymptotic limits of the NeF^+ potential energy curves, 0.25 and 0.17 eV. The other electronic state that shows binding is the lowest $^1\Pi$, but the dissociation energy of this state is only 0.18 eV.

TABLE III. Crossing points for the potential curves of NeF^+.

	Unshifted[a]		Shifted[b]	
	R^c	ΔE^d	R^c	ΔE^d
$^1\Sigma^+$-$^3\Pi$	1.533	1.252	1.564	1.053
$^1\Sigma^+$-$^3\Sigma^-$	1.701	1.639	1.726	1.458
$^1\Pi$-$^3\Sigma^-$	1.544	3.374	1.570	2.996

[a]From theoretical potential curves.
[b]Obtained with curves shifted to fit the exponential asymptotes.
[c]Ne-F distance at crossing in angstroms.
[d]Energy at crossing relative to $Ne(^1S)+F^+(^3P)$ in eV.

The interaction between the F^+ ion and the induced dipole moment of the neon atom might be expected to cause a weak minimum on the lowest $^3\Pi$ and $^3\Sigma^-$ curves. However, these curves are found to be purely repulsive. The present basis sets are believed to account reasonably well for the polarization effects. With a roughly comparable $(6s,4p,3d)$ basis set, Maroulis and Bishop[25] obtained a dipole polarizability of 2.13 for neon, the experimental value being 2.67. Nelin *et al.*[26] have shown that the

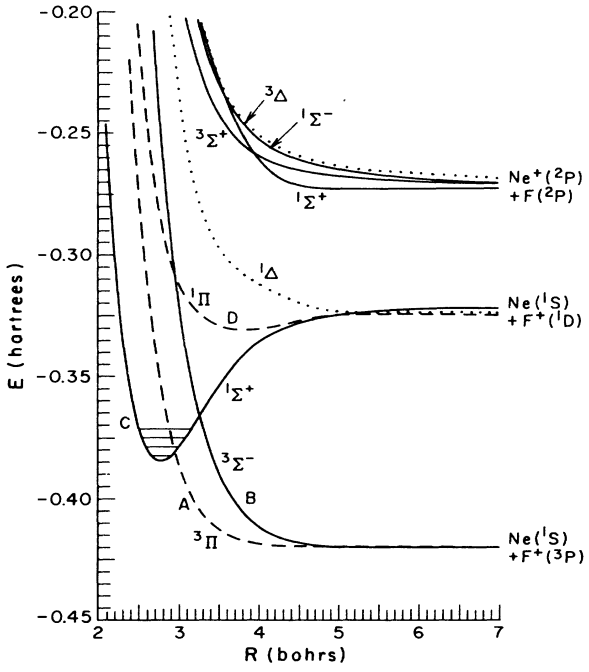

FIG. 4. Potential energy curves for the NeF^+ system: ——, Σ states; — — —, Π states; · · · ·, Δ states. Altogether 18 molecular states correlate to the four lowest atomic terms of $Ne+F^+$ and Ne^++F, of which nine are shown here. Others appear to be repulsive. Curves labeled A—D are involved in inelastic transitions.

TABLE II. Potential curves for NeF^+ (unshifted). Values given should be added to 227, except those marked by an asterisk which are added to 226. The result is minus the energy of the state. Values are in units of a.u.

R	$1\,^3\Pi$	$1\,^3\Sigma^-$	$1\,^1\Sigma^+$	$1\,^1\Pi$	$1\,^1\Delta$	$1\,^3\Sigma^+$	$1\,^3\Delta$	$1\,^1\Sigma^-$	$2\,^1\Sigma^+$	$2\,^3\Pi$	$2\,^1\Pi$
2.20			0.287 508								
2.30			0.322 575								
2.40	0.219 898		0.346 366	0.144 978	0.910 292*						
2.45	0.246 727		0.354 927	0.172 066	0.955 607*						
2.50	0.270 103		0.361 692	0.195 467	0.995 852*	0.996 264*	0.861 933*				
2.55	0.290 365		0.366 837	0.215 611	0.031 467	0.025 101					
2.60	0.307 991	0.154 119	0.370 592	0.232 878	0.063 068	0.050 739					
2.65	0.323 221		0.373 192	0.247 625	0.091 131	0.073 465					
2.70	0.336 424		0.374 744	0.260 170	0.116 087	0.093 718					
2.75	0.347 860		0.375 420	0.270 800	0.138 285	0.111 664	0.036 854				
2.80	0.357 744	0.254 667	0.375 338	0.279 747	0.158 043	0.127 649					
2.85	0.366 302		0.374 672	0.287 235	0.175 640	0.141 838					
2.90	0.373 745	0.289 839	0.373 484	0.293 467	0.191 313	0.154 455					
2.95	0.380 146		0.371 853	0.298 616		0.165 688					
3.00	0.385 721	0.317 694	0.369 888			0.175 671	0.133 581	0.134 991	0.151 695	0.154 217	0.151 140
3.10		0.339 729									
3.20		0.357 128		0.313 021							
3.25	0.404 222		0.357 254			0.211 567	0.186 874			0.192 827	0.191 148
3.30		0.370 871									
3.50	0.413 088	0.390 244	0.344 551			0.231 401	0.216 017	0.216 713	0.217 896	0.214 077	0.213 040
4.00	0.418 869	0.412 123	0.326 748			0.248 859	0.239 983	0.241 884		0.232 401	0.232 974
4.50	0.419 500	0.418 253									
5.00	0.419 436	0.419 777	0.315 344			0.257 256		0.247 118	0.262 487	0.238 313	0.240 568
10.00	0.418 442	0.419 558	0.315 075					0.260 998	0.260 998	0.244 054	0.244 049

TABLE IV. Spectroscopic constants for $F_2(X\,^1\Sigma_g^+)$ and $NeF^+(1\,^1\Sigma^+)$.[a]

	F_2		NeF^+
	Calc.	Expt.[b]	Calc.
r_e (Å)	1.419	1.412	1.465
D_e (eV)	1.598		1.644
D_0 (eV)	1.541	1.602	1.591
ω_e (cm^{-1})	923.8	916.6	861.7
$\omega_e x_e$ (cm^{-1})	9.38	11.24	7.28
$\omega_e y_e$ (cm^{-1})	−0.94	−0.11	−0.33
B_e (cm^{-1})	0.881	0.890	0.805
α_e (cm^{-1})	11.7×10^{-3}	13.8×10^{-3}	9.6×10^{-3}
γ_e (cm^{-1})	-6.7×10^{-4}	1.2×10^{-4}	-2.0×10^{-4}
d_e (cm^{-1})	3.09×10^{-6}	3.3×10^{-6}	2.8×10^{-6}
Band origins[c]			
$\Delta G_{1/2}$ (cm^{-1})	901.5	894	845.7
$\Delta G_{3/2}$ (cm^{-1})	875.3	870	829.2
$\Delta G_{5/2}$ (cm^{-1})	841.7	846	808.2

[a]Calculated from a numerical solution of the radial Schrödinger equation, using $v=0$–4 and $J=0$–20.
[b]Experimental values from Ref. 27.
[c]Experimental values from Ref. 28.

correlation effects are not very pronounced in this case and the present active space covers most of the correlation contribution. Therefore we conclude that the repulsive forces dominate the attractive ones at intermediate internuclear distances.

C. Curve crossings and electronic transitions

Several curve crossings are found in this calculation, and the computed crossing points for both the shifted and unshifted energy curves are listed in Table III.

1. Predissociation

As already mentioned, both the $^3\Pi$ and $^3\Sigma^-$ curves cross the binding $^1\Sigma^+$ state near the minimum. Spin-orbit coupling terms in the Hamiltonian produce matrix elements that connect these states, and induce electronic transitions. Therefore the rovibrational levels associated with the $^1\Sigma^+$ electronic state are not truly bound, but undergo dissociation with a finite lifetime. This lifetime is *extremely* sensitive to the exact relative positions of the potential energy curves. If the crossing occurs in a classically forbidden region of the nuclear motion, then the state can have a long lifetime with respect to dissociation, but if it occurs in a classically allowed region, the state will have a short lifetime.

For example, according to Fig. 4, the $^3\Sigma^-$ and $^1\Sigma^+$ curves cross at about 1.7 Å; the lowest five vibrational states of the $^1\Sigma^+$ state have their outer turning points at smaller distances, so the crossing point is in a classically forbidden region, and the lowest states would have long lifetimes with respect to this transition (up to 10^{10} or more vibrational periods). On the other hand, the higher vibrational states ($v\gtrsim5$) have outer turning points at larger distances than the crossing point, and these states will have short lifetimes for this transition (~20 to 100 vibrational periods).

The $^3\Pi$ state crosses the $^1\Sigma^+$ state near 1.5 or 1.6 Å; this is in the classically allowed region of the vibrational states $v\geq1$, but slightly in the classically forbidden region of the $v=0$ state. Therefore only this $v=0$ vibrational state could have an extended lifetime, and it might be as small as a thousand or so vibrational periods. However, a small shift in the relative positions of these curves would dramatically alter this conclusion. An upward shift of the $^3\Pi$ relative to the $^1\Sigma^+$ would increase the lifetime by a large factor, a small downward shift would decrease the lifetime, while a larger downward shift would again increase the lifetime. Therefore no unambiguous conclusion can be drawn about the stability of NeF^+ from this calculation. (We recall that the experimental results are also inconclusive.)

2. Inelastic collisions

The same curve crossings, together with the $^3\Sigma^-$-$^1\Pi$ crossing mediate the inelastic $^3P\leftrightarrow{}^1D$ transitions which are seen experimentally, and these will be discussed in more detail in later sections.

3. Charge transfer

Charge transfer at low energies is known to be very improbable unless there is a degeneracy or near degeneracy that mediates the transition. However, a relevant degeneracy has not yet been identified. The obvious candidates ($1\,^3\Pi$–$2\,^3\Pi$), ($1\,^3\Sigma^-$–$2\,^3\Sigma^-$), ($1\,^1\Pi$–$2\,^1\Pi$), ($1\,^1\Delta$–$2\,^1\Delta$) have been examined and in every case the calculation gives a higher state which is very repulsive and does not approach the lower state. Presently the experimentally observed charge transfer is not explained.

In Secs. IV and V we examine the inelastic $^3P\leftrightarrow{}^1D$ excitations in more detail. First we obtain an estimate of the spin-orbit matrix elements, and then we give a semiquantal description of the collision process.

IV. SPIN-ORBIT COUPLING MATRIX ELEMENTS

As discussed above, excitations and deexcitations between $F^+(^3P)$ and $F^+(^1D)$ occur near the crossings seen in Fig. 4. For convenience we label the relevant molecular terms A,B,C,D, according to Table V. Transitions occur through spin-orbit interactions connecting A to C, B to

TABLE V. Labels for terms and states.

Term label	Symmetry	$\lvert S\,\Sigma\,L\,\Lambda\rangle$	Ω	State label
A	$1\,^3\Pi$	$\lvert 1-111\rangle$	0	A_1
		$\lvert 111-1\rangle$	0	A_2
B	$1\,^3\Sigma^-$	$\lvert 1010\rangle$	0	B_0
		$\lvert 1110\rangle$	1	B_+
		$\lvert 1-110\rangle$	−1	B_-
C	$1\,^1\Sigma^+$	$\lvert 0020\rangle$	0	C
D	$1\,^1\Pi$	$\lvert 0021\rangle$	1	D_+
		$\lvert 002-1\rangle$	−1	D_-

C, and B to D. Accurate calculation of these matrix elements would be a large computational task, for which we do not possess the programs. However, they can easily be estimated using a kind of linear combination of atomic orbitals (LCAO) approximation. We assume that near the crossings (around $3a_0$) the spin-orbit matrix elements are close to the values obtained for the separated atoms, and we use measured spin-orbit splittings to calculate them. This can be partly justified from the fact that spin-orbit matrix elements are primarily determined by those parts of the electronic wave functions that are close to the nuclei, and such parts of the wave functions are least distorted by the molecular fields.

The spin-orbit operator for several electrons interacting with several nuclei is

$$H'=\frac{1}{2m^2c^2}\sum_{i,\alpha}\frac{1}{r_i}\frac{\partial V_\alpha(r_i)}{\partial r_i}\mathbf{l}_i\mathbf{s}_i\ , \tag{3a}$$

where $V_\alpha(r_i)$ is a central field associated with nucleus α. Following standard notation, we write

$$\xi(r)=\frac{1}{2m^2c^2}\sum_{\alpha}\frac{1}{r}\frac{\partial V_\alpha(r)}{\partial r}\ . \tag{3b}$$

The F^+ ion has four electrons outside a closed shell, but it is simpler to say that it has two holes in the p shell. Then the spin-orbit operator has the same form, but now i labels a hole rather than an electron, and the sign of the effective central potential is changed.

When this operator acts upon states characterized by quantum numbers $|S\Sigma L\Lambda\rangle$ (where Σ and Λ are components of electronic spin and orbital angular momentum along the internuclear axis) it connects them subject to the selection rules

$$\begin{aligned}&\Delta L=\pm1,0\ ,\\&\Delta S=\pm1,0\ ,\\&\Delta\Lambda=\pm1,0\ ,\\&\Delta\Sigma=\pm1,0\ ,\\&\Delta\Omega=0\end{aligned} \tag{4}$$

(here $\Omega=\Sigma+\Lambda$) corresponds to the component of $L+S$). In molecules, L is not generally a good quantum number, but, consistent with our method of obtaining the required matrix elements by examination of the separated atoms, we treat it as if it were a good quantum number, and we take the value of L for any molecular state to be the value that emerges at large R. With this approximation, the estimation of the matrix elements becomes a standard exercise in angular-momentum unscrambling, and we use formulas given in Chapter 3 of Condon and Shortley (CS).[29] The relevant terms and states are listed in Table V.

The C term ($1\,^1\Sigma^+$) consists of only one state, for which the quantum numbers $|S\Sigma L\Lambda\rangle$ are $|0020\rangle$. $L=2$ is obtained from the fact that it goes to a D term at large R. Since Ω for this state is equal to zero, this C state is coupled only to those A states and B states for which Ω is also equal to zero. The relevant B state is denoted B_0, and its quantum numbers $|S\Sigma L\Lambda\rangle$ are $|1010\rangle$. We therefore need the matrix element

$$\begin{aligned}\langle B_0|H'|C\rangle&=\left\langle B_0\left|\sum_i\xi(r_i)\mathbf{l}_i\mathbf{s}_i\right|C\right\rangle\\&=\sum_i\langle B_0^r|\xi(r_i)|C^r\rangle\langle1010|\mathbf{l}_i\mathbf{s}_i|0020\rangle\ ,\end{aligned} \tag{5}$$

where $|B_0^r\rangle$ and $|C^r\rangle$ are the radial parts of the wave function. The angular parts are evaluated in Condon and Shortley (p. 63, the second and sixth of the set of equations numbered 9^311)

$$\begin{aligned}\langle1010|\mathbf{l}_i\mathbf{s}_i|0020\rangle&=\langle10|\mathbf{l}_i|20\rangle\cdot\langle10|\mathbf{s}_i|00\rangle\\&=2(1{:}l_i{:}2)(1{:}s_i{:}0)\ .\end{aligned} \tag{6}$$

Since there are two equivalent holes, we obtain

$$\langle B_0|H'|C\rangle=(2\zeta_{BC})2(1{:}l{:}2)(1{:}s{:}0)\ , \tag{7}$$

where

$$\zeta_{BC}=\langle B^r|\xi(r)|C^r\rangle\ . \tag{8}$$

For the A term we say that $L=1$, since it correlates to ^3P. There are six A states, but only two of these (denoted A_1 and A_2) have $\Omega=0$, so only these are coupled to C. Their quantum numbers $|S\Sigma L\Lambda\rangle$ are $|1-111\rangle$ and $|1111-1\rangle$. The matrix elements $\langle A_1|H'|C\rangle$ and $\langle A_2|H'|C\rangle$ are equal in magnitude, and either can be evaluated using the first and fifth of Eqs. 9^311 (CS p. 63),

$$\begin{aligned}\langle A_1|H'|C\rangle&=\sum_i\langle A_1^r|\xi(r_i)|C^r\rangle\langle1-111|\mathbf{l}_i\mathbf{s}_i|0020\rangle\\&=2\zeta_{AC}\langle11|\mathbf{l}_i|20\rangle\cdot\langle1-1|\mathbf{s}_i|00\rangle\\&=2\zeta_{AC}(1{:}l{:}2)(1{:}s{:}0)\ .\end{aligned} \tag{9}$$

Like term A, term D is assigned the quantum number $L=2$, but $\Lambda=\pm1$, leading to $\Omega=\pm1$, so it interacts with the corresponding components in the B term. We have

$$\begin{aligned}&\langle B_+|H'|D_+\rangle\\&\quad=\sum_i\langle B_+^r|\xi(r_i)|D_+^r\rangle\langle1110|\mathbf{l}_i\mathbf{s}_i|0021\rangle\\&\quad=2\langle B_+^r|\xi(r_i)|D_+^r\rangle\langle10|\mathbf{l}_i|21\rangle\cdot\langle11|\mathbf{s}_i|00\rangle\\&\quad=2\zeta_{BD}(1{:}l{:}2)(1{:}s{:}0)\sqrt{3}\ .\end{aligned} \tag{10}$$

Next we need to evaluate the reduced matrix elements $(1{:}l{:}2)$ and $(1{:}s{:}0)$. The first of these involves a matrix element of a one-electron orbital angular momentum operator between states in which the total orbital angular momentum is respectively $\hbar$ and $2\hbar$. This latter state, of course, arises from the fact that F^+ possesses two holes in p orbitals, each of which has an angular momentum of one $\hbar$; therefore $(1{:}l{:}2)$ is a special case of a matrix element

$$(1{:}l{:}2)\equiv(l_1,l_2,L-1{:}l_1{:}l_1,l_2,L) \tag{11}$$

with $l_1=l_2=1$, $L=2$. This matrix element is evaluated

in Eqs. $10^3$2b and $10^3$2b′ of CS (p. 66); it is

$$(l_1,l_2,L-1{:}l_1{:}l_1,l_2,L) = [P(L)Q(L-1)/(4L^2-1)]^{1/2}/2L \ , \quad (12)$$

where

$$P(L)=(L-l_1+l_2)(L+l_1+l_2+1)=10 \ , \quad (13)$$

$$Q(L-1)=(l_1+l_2-L+1)(L-1+l_1-l_2+1)=2 \ .$$

Hence

$$(1{:}l{:}2)=1/(2\sqrt{3}) \ . \quad (14)$$

Similarly $(1{:}s{:}0)$ is a special case of a matrix element

$$(1{:}s{:}0)=(s_1,s_2,S{:}s_1{:}s_1,s_2,S-1) \quad (15)$$

with $s_1=s_2=\frac{1}{2}$, $S=1$. This matrix element is evaluated in the same way,

$$(s_1,s_2,S{:}s_1{:}s_1,s_2,S-1) = [P(S)Q(S-1)/(4S^2-1)]^{1/2}/2S \ ,$$

$$P(S)=(S-s_1+s_2)(S+s_1+s_2+1)=3 \ , \quad (16)$$

$$Q(S-1)=(s_1+s_2-S+1)(S-1+s_1-s_2+1)=1 \ , \quad (17)$$

so

$$(1{:}s{:}0)=\tfrac{1}{2} \ . \quad (18)$$

It therefore follows that the product $(1{:}l{:}2)(1{:}s{:}0)$ which appears in all of the matrix elements above is equal to

$$(1{:}l{:}2)(1{:}s{:}0)=1/(4\sqrt{3}) \ . \quad (19)$$

The remaining unknown quantities are the radial factors ζ_{AC}, ζ_{BC}, and ζ_{BD}. Within the SCF approximation in the separated atom limit, these are all equal, and their common value determines the spin-orbit splitting in the ^3P term. The spin-orbit coupling operator commutes with the total angular momentum, so atomic energy levels are characterized by quantum numbers $|SLJM\rangle$, and the energy level formula is

$$E'=\langle SLJM|H'|SLJM\rangle = 2\zeta\langle SLJM|l_1\cdot s_1|SLJM\rangle \ , \quad (20)$$

where ζ is again the radial part of the matrix element. Now $l_1 s_1$ is an operator of the type discussed on p. 71 of CS, and we find from the first of their equations $12^3$2,

$$\langle SLJM|l_1 s_1|SLJM\rangle = (S{:}s_1{:}S)(L{:}l_1{:}L) \times \tfrac{1}{2}[J(J+1)-L(L+1)-S(S+1)] \ . \quad (21)$$

The reduced matrices appearing in this formula are evaluated on p. 64, Eq. $10^3$2a. In the present case (^3P) we have $S=1$, $L=1$, $s_1=s_2=\frac{1}{2}$, $l_1=l_2=1$, so

$$(S{:}s_1{:}S)=\tfrac{1}{2} \ , \quad (L{:}l_1{:}L)=\tfrac{1}{2} \ . \quad (22)$$

Therefore the spin-orbit coupling energy is equal to

$$E'=(\tfrac{1}{2}\zeta)(\tfrac{1}{2})[J(J+1)-L(L+1)-S(S+1)] \quad (23)$$

and the splitting between state J and state $J-1$ is

$$\Delta E'=E'_J-E'_{J-1} = \tfrac{1}{2}\zeta J \ . \quad (24)$$

Measured values of these energy levels are given in Charlotte Moore's tables.[22] For $J=2,1,0$, respectively, the values are 0.0, 341.8, and 490.6 cm^{-1}. From this we conclude that $\zeta=2\Delta E'/J$ must be 320 ± 20 cm^{-1}.

Finally we combine the above results, using the above-mentioned approximation that all ζ's have the same value. The result is

$$\langle A_1|H'|C\rangle = 2\zeta/(4\sqrt{3}) = 92.4 \text{ cm}^{-1} = 4.21\times10^{-4} \text{ hartrees} \ ,$$
$$\langle B_0|H'|C\rangle = 2\zeta\times2/(4\sqrt{3}) = 184.8 \text{ cm}^{-1} = 8.42\times10^{-4} \text{ hartrees} \ ,$$
$$\langle B_+|H'|D_+\rangle = (2\zeta/4\sqrt{3})\sqrt{3} = 160 \text{ cm}^{-1} = 7.29\times10^{-4} \text{ hartrees} \ . \quad (25)$$

The most significant approximation made in this analysis is the use of the same asymptotic value of ζ for all matrix elements. This probably leads to overestimation of these couplings. We think that the correct values lie somewhere between 0.7 and 1.0 times the values given above.

V. DYNAMICS OF INELASTIC TRANSITIONS

We now examine in more detail the inelastic (^3P-^1D) transitions that are observed at small angles.

A. Theoretical methods

A complete quantum-mechanical description of these collisions would involve an expansion of the full wave function for electrons and nuclei in a basis set that would include at least the fourteen electronic states that correlate to the atomic ^3P and ^1D terms. Significant couplings among these states occur in two regions: near the curve crossings, where $A\leftrightarrow C$, $B\leftrightarrow C$, and $B\leftrightarrow D$ transitions take place, and at large separations, where the competition among electrostatic, spin-orbit, and rotational couplings

causes the states to lock onto the internuclear axis and change from space-fixed atomic to rotating molecular states. This complete description would involve integration of many coupled differential equations in each partial wave. However, such a complete and complicated description is neither necessary nor desirable at present. The available experimental results can be interpreted much more easily by the use of the simplifying approximations listed below.

(1) The rotational couplings at large R are independent of the curve crossings at smaller R. The regions in which each of these couplings are important are well separated, and one set of transitions is complete before the other begins to occur. Because in this case the spin-orbit interactions are small, the coupling problem at large R can be solved using the sudden approximation.[30] Independent of that approximation, however, since the atomic states within each atomic term are statistically populated, it follows that the initial or incident population of molecular states will also be statistical. Thus we may think of the initial conditions associated with the $^3P \rightarrow {}^1D$ excitation as being an incoherent mixture with $\frac{2}{3}$ of the atoms entering the $^3\Pi$ term and $\frac{1}{3}$ of the atoms entering the $^3\Sigma$ term. Similarly, initial conditions associated with the $^1D \rightarrow {}^3P$ deexcitation are an incoherent mixture of $\frac{2}{5}\,{}^1\Delta$, $\frac{2}{5}\,{}^1\Pi$, and $\frac{1}{5}\,{}^1\Sigma^+$.

(2) The change of angular momentum of the electrons ($L=1 \leftrightarrow L=2$) does not significantly affect the relative motion of the atoms, and the relative angular momentum is essentially conserved. It follows that the wave functions for relative motion of the atoms can be expanded in Legendre polynomials, and the amplitude for scattering to angle θ if the initial electronic state is m and the final state is n is given by

$$f_{m\rightarrow n}(\theta)=(2ik_m)^{-1}\sum_N (2N+1)P_N(\cos\theta)(\mathscr{S}^N_{mn}-\delta_{mn}) \ . \tag{26}$$

Here k_m is the wave vector associated with the initial state, and $\mathscr{S}^N_{mn}$ is the element of the $\mathscr{S}$ matrix for the Nth partial wave. This approximation is justified by the fact that the relevant values of N are in the hundreds, while the change of N is only one unit.

(3) The $\mathscr{S}$ matrix is calculated by treating the relative atomic motion in each partial wave semiclassically. This combination of semiclassical approximation in each partial wave together with numerical summation over N is called a semiquantal approximation, and a general semiquantal framework for inelastic processes was developed and implemented in Refs. 31 and 32. With this approximation, the $\mathscr{S}$ matrix is given by

$$\mathscr{S}^N_{mn}=\exp[i(\eta^N_m+\eta^N_n)](\underline{G}^N\underline{\tilde{G}}^N)_{mn} \ , \tag{27}$$

where η_n is the WKB phase shift associated with elastic scattering on the nth state. The matrix $\underline{G}$ is the half-collision evolution matrix

$$\underline{c}(\infty)=\underline{G}\underline{c}(0) \tag{28a}$$

associated with the electronic amplitudes which satisfy the "classical trajectory equations"

$$i\hbar\frac{d}{dt}\underline{c}(t)=(\underline{h}+v\underline{P})\underline{c}(t) \ . \tag{28b}$$

The forms of $\underline{h}$ and $\underline{P}$ depend upon the representation chosen. In the present case, the potential curves shown in Fig. 4 constitute a "diabatic" representation, in which the spin-orbit terms in the Hamiltonian are nondiagonal, but P-matrix elements vanish between singlet and triplet states. The corresponding adiabatic representation is obtained by diagonalizing the full Hamiltonian including spin-orbit couplings. Our programs had been set up to perform calculations in this adiabatic representation.

(4) The three curve crossings are independent, and the couplings are sufficiently weak that the total excitation probability can be obtained by adding excitation amplitudes for each crossing. Thus we reduce the description to three separate two-state crossing problems. Our calculations indicate that the transition probability at each crossing is less than 0.05, and that the crossings are well separated, so this approximation should have less than 5% error.

(5) For small angular momentum quantum numbers ($N<300$ or so, depending on the pair of states involved), when the classical turning point is well inside the crossing point, the Landau-Zener formula gives an adequate approximation to the $\underline{G}$ matrix. For larger N, where the turning point is close to the crossing point, a quadratic model described in Ref. 32 can be used, and the $\underline{G}$ matrix is obtained by integration of a pair of coupled equations which are a special case of (28b).

Each of the above approximations is well justified in the present context. They greatly simplify the calculations and reduce the computer time required. In addition, they directly provide a semiclassical interpretation of the results. For example, semiclassical deflection functions are given by derivatives such as

$$\theta(b)=\frac{d}{dL}[(\eta_1+\eta_2)\pm(\Gamma_1+\Gamma_2)] \ , \tag{29}$$

where Γ_1 and Γ_2 are phases associated with the two-state $\underline{G}$ matrix.[32]

Additional details regarding the methods used are given in Refs. 31 and 32.

B. Results

Deflection functions associated with the $B \leftrightarrow C$ ($^3\Sigma^- \leftrightarrow {}^1\Sigma^+$) crossing are shown in Fig. 5, and the associated differential cross section is shown in Fig. 6. These plots have the following interpretation. The F^+ approaches the Ne with a c.m. energy of 9.75 eV and an impact parameter b, such that $N=(2\mu E)^{1/2}b/\hbar$. The F^+ is initially in the $C(^1\Sigma^+)$ molecular state, having come from the atomic ^1D state, and after the collision the system is in the $B(^3\Pi)$ state going out to the atomic ^3P. Transitions primarily occur near the crossing, and they can take place either on the incoming or outgoing part of the trajectory. Hence there are two paths leading from the initial state to the final state, and these paths give the scattering angles shown. The deflection functions shown in Fig. 5 refer to the c.m. frame. On the other hand, the differential cross section shown in Fig. 6 refers to the laboratory frame.

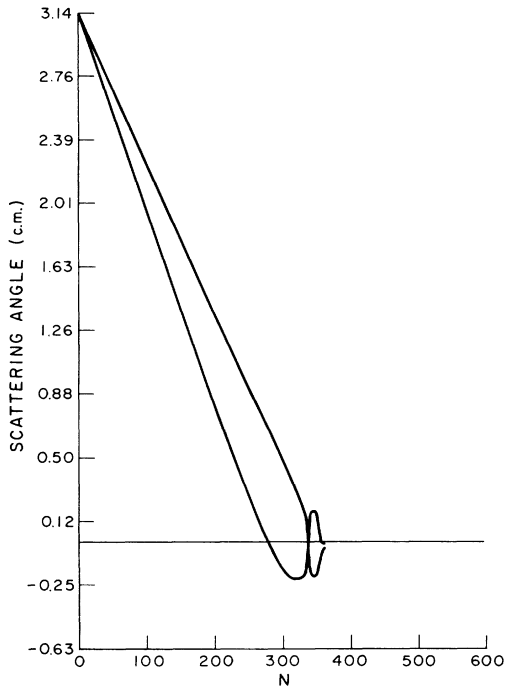

FIG. 5. Deflection functions associated with the $B \rightarrow C$ transition. The scattering angle is given in radians in the center-of-mass (c.m.) frame. N is the angular momentum quantum number for the heavy particles.

For $N=0$, the F^+ is scattered backwards, to $\theta=\pi$, and as N increases the scattering angles decrease. One of them passes through zero and then reaches a minimum of about -0.21 rad ($-12°$) at $N \sim 315$. This deflection function arises from deexcitations that occur on the outgoing part of the trajectory. The other deflection function arises from deexcitations that occur on the incoming part of the trajectory. In this case the F^+ ion moves on the repulsive B curve for a longer time, and it is scattered to larger angles. The two deflection functions pass through each other at $N \sim 340$, where it happens that they are both close to $\theta=0$. (For $N > 340$ the deflection functions have curious but physically irrelevant behavior, because the transition probability is exponentially small in that region.[32])

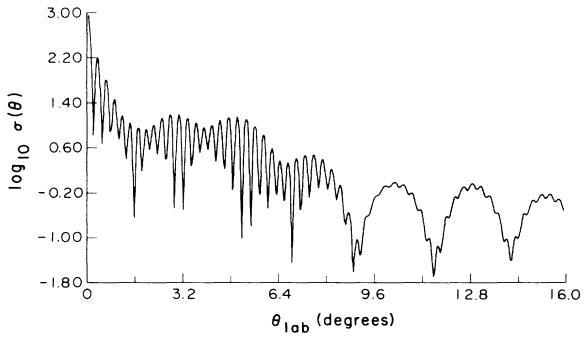

FIG. 6. Differential cross section for $C \rightarrow B$ transition (laboratory frame). $\sigma(\theta)$ is given in bohr^2/steradian.

The minimum in the lower branch of the deflection function gives rise to a "rainbow."[32,33] The classical formula for the differential cross section is

$$\sigma_{m \rightarrow n}(\theta) = P_{m \rightarrow n}(b(\theta)) \frac{b(\theta) db}{\sin\theta \, d\theta} , \tag{30}$$

where $P_{m \rightarrow n}$ is the transition probability. This classical formula diverges when $d\theta/db = 0$, and for angles outside the rainbow it gives no contribution. In semiclassical mechanics the singularity is spread out into an Airy function. The rainbow angle in the laboratory frame is about 6°; in Fig. 6 one sees that in this region the differential cross section is rapidly decreasing with increasing angle (note the logarithmic scale).

For scattering angles larger than the rainbow angle, there are two paths, or two different impact parameters that lead to the same final scattering angle. Hence the differential cross section shows smooth oscillations representing interference of amplitude associated with these paths. At angles smaller than the rainbow angle, there are four different paths leading to the same final scattering angle, and a much more complicated interference pattern is found there.

Most important, the deflection functions pass through zero at $N \sim 275$ and at $N \sim 340$. At this point the classical formula for the differential cross section gives another singularity ($\sin\theta = 0$) known as the "forward glory." The semiquantal formula gives a finite but very large differential cross section at $\theta=0$. It is this small-angle peak that is seen in the experiments.

The other two curve crossings provide two other routes to deexcitation. Differential cross sections for them have also been calculated, and similar phenomena are seen. To obtain the total differential cross section for $^1D \rightarrow {}^3P$, we added these calculated cross sections, incorporating the statistical factors mentioned earlier. (Note also that the $C \rightarrow A$ transition counts twice, because there are two A states coupled to the C state.) The result is wildly oscillatory and small at most angles, but sharply peaked at $\theta=0$.

Finally, we convoluted this theoretical differential cross section with a Gaussian function having a FWHM of 1.66°,

$$\sigma_{\text{conv}}(\theta) = \int \sigma_{\text{calc}}(\theta') g(\theta' - \theta) \sin\theta' d\theta' . \tag{31}$$

The result is shown in Fig. 3 along with the experimental measurements. The two results were normalized to match at $\theta=0$. They agree with each other beautifully at all other angles. One has to admit, however, that this agreement comes more from the convolution procedure than from the scientifically interesting parts of the theory. The basic conclusion of the theoretical calculation is that the differential cross section is *very* sharply peaked in the forward direction, having FWHM on the order of 0.1°.

VI. CONCLUSIONS

Observations of collisions of F^+ with Ne show that $^1D \leftrightarrow {}^3P$ transitions take place such that an observable current is seen in the forward direction only. Calculations of the potential energy curves show the presence of three

curve crossings that mediate these transitions. A semiquantal calculation shows that the sharp peaking of the cross section in the forward direction is related to a glory effect.

Two other interesting questions are raised by this work, but are not yet definitely answered. Observations show that these collisions can also lead to charge exchange, but at the moment a curve crossing that would mediate this process has not been identified. Also some evidence has been found that the molecular ion NeF^+ may be stable or metastable, but neither theory nor experiment establishes this conclusively.

ACKNOWLEDGMENTS

J.B.D. and R.S. acknowledge support from the National Science Foundation Chemistry Section and India-U.S. Exchange of Scientists Program. J.B.D. also acknowledges financial support of the Joint Institute for Laboratory Astrophysics (JILA) Visiting Fellow Program.

*Present address: Joint Institute for Laboratory Astrophysics, University of Colorado and National Bureau of Standards, Boulder, Colorado 80309-0440.

[1]L. G. Piper, J. E. Velazco, and D. W. Setser, J. Chem. Phys. **59**, 3323 (1973).

[2]J. E. Velazco, J. H. Kolts, and D. W. Setser, J. Chem. Phys. **65**, 3468 (1976).

[3]J. Tellinghuisen, A. K. Hays, J. M. Hoffmann, and C. C. Tisome, J. Chem. Phys. **65**, 4473 (1976).

[4]D. L. King, L. G. Piper, and D. W. Setser, J. Chem. Soc. Faraday Trans. III **73**, 177 (1977).

[5]M. Rokni, J. H. Jacobs, and J. A. Mangano, Phys. Rev. A **16**, 2216 (1977).

[6]R. E. Olson and B. Liu, Phys. Rev. A **17**, 1568 (1978).

[7]T. H. Dunning, Jr. and P. J. Hay, J. Chem. Phys. **66**, 3767 (1977), and references therein.

[8]J. S. Cohen, W. R. Wadt, and P. J. Hay, J. Chem. Phys. **71**, 2955 (1979), and references therein.

[9]H. P. Watkins, N. E. Sondergaard, and W. S. Koski, Radiochim. Acta **29**, 87 (1981).

[10]J. H. Holloway, *Noble Gas Chemistry* (Methuen, London, 1968).

[11]A. Henglein and G. A. Muccini, Angew. Chem. **72**, 630 (1960).

[12]I. Kuen and F. Howorka, J. Chem. Phys. **70**, 595 (1979).

[13]H. P. Watkins and W. S. Koski, Chem. Phys. Lett. **77**, 470 (1981).

[14]J. Berkowitz and W. A. Chupka, Chem. Phys. Lett. **7**, 447 (1970).

[15]K. Wendell, C. A. Jones, J. J. Kaufman, and W. S. Koski, J. Chem. Phys. **63**, 750 (1975).

[16]K.-C. Lin, R. J. Cotter, and W. S. Koski, J. Chem. Phys. **61**, 905 (1974).

[17]B. O. Roos, Int. J. Quantum Chem. S **14**, 175 (1980); P. E. M. Siegbahn, A. Heiberg, B. Roos, and B. Levy, Phys. Scr. **21**, 323 (1980); B. O. Roos, P. R. Taylor, and P. E. M. Siegbahn, Chem. Phys. **48**, 157 (1980).

[18]B. Levy and G. Berthier, Int. J. Quantum Chem. **2**, 307 (1968); F. Grein and T. C. Chang, Chem. Phys. Lett. **12**, 44 (1971); F. Grein and A. Banerjee, Int. J. Quantum Chem. S **9**, 147 (1975); F. Grein and G. Banerjee, J. Chem. Phys. **66**, 1054 (1977).

[19]I. Shavitt, Int. J. Quantum Chem. S **11**, 131 (1977); S **12**, 5 (1978).

[20]M. R. A. Blomberg and P. E. M. Siegbahn, Chem. Phys. Lett. **81**, 4 (1981).

[21]F. B. van Duijneveldt, IBM Report RJ945, 1971 (unpublished).

[22]R. Ahlrichs, J. Chem. Phys. **62**, 1235 (1975).

[23]C. E. Moore, *Atomic Energy Levels*, Natl. Bur. Stand. (U.S.) Circ. No. 467 (U.S. GPO, Washington, D.C., 1949), Vol. 1.

[24]J. F. Liebman and L. C. Allen, J. Am. Chem. Soc. **92**, 3539 (1970).

[25]G. Maroulis and D. M. Bishop, Chem. Phys. Lett. **114**, 182 (1985).

[26]C. Nelin, B. O. Roos, A. J. Sadlej, and P. E. M. Siegbahn, J. Chem. Phys. **77**, 3607 (1982).

[27]K. P. Huber and G. Herzberg, *Constants of Diatomic Molecules* (Van Nostrand Reinhold, New York, 1979).

[28]E. A. Colborn, M. Dagenais, A. E. Douglas, and J. W. Raymonda, Can. J. Phys. **54**, 1343 (1976).

[29]E. U. Condon and G. H. Shortley, *Theory of Atomic Spectra* (Cambridge University Press, Cambridge, 1963).

[30]W. R. Thorson, J. Chem. Phys. **50**, 1702 (1969).

[31]J. B. Delos, W. R. Thorson, and S. K. Knudson, Phys. Rev. A **6**, 709 (1972); J. B. Delos and W. R. Thorson, *ibid.* **6**, 720 (1972).

[32]J. B. Delos and W. R. Thorson, Phys. Rev. A **6**, 728 (1972); J. B. Delos, *ibid.* **9**, 1626 (1974).

[33]K. A. Ford and J. A. Wheeler, Ann. Phys. (N.Y.) **7**, 259 (1959); **7**, 287 (1959); R. E. Olson and F. T. Smith, Phys. Rev. A **3**, 1607 (1971); S. M. Bobbio, R. L. Champion, and L. D. Doverspike, *ibid.* **7**, 526 (1973); G. A. L. Delvigne and J. Los, Physica **59**, 61 (1972).

[34]R. B. Bernstein, in *Molecular Beams*, Vol. 10 of *Advances in Chemical Physics*, edited by J. Ross (Interscience, New York, 1966), p. 114.